Laitinen, Antti; Kumar, Manohar; Hakonen, Pertti J.

Weak antilocalization of composite fermions in graphene

Published in:
Physical Review B

DOI:
10.1103/PhysRevB.97.075113

Published: 08/02/2018

Document Version
Publisher's PDF, also known as Version of record

Please cite the original version:
Laitinen, A., Kumar, M., & Hakonen, P. J. (2018). Weak antilocalization of composite fermions in graphene. Physical Review B, 97(7), 1-5. [075113]. https://doi.org/10.1103/PhysRevB.97.075113

Weak antilocalization of composite fermions in graphene

Antti Laitinen, Manohar Kumar, and Pertti J. Hakonen
Low Temperature Laboratory, Department of Applied Physics, Aalto University, Espoo, Finland

(Received 18 December 2016; published 8 February 2018)

We demonstrate experimentally that composite fermions in monolayer graphene display weak antilocalization. Our experiments deal with fractional quantum Hall (FQH) states in high-mobility, suspended graphene Corbino disks in the vicinity of $\nu = 1/2$. We find a strong temperature dependence of conductivity σ away from half filling, which is consistent with the expected electron-electron interaction-induced gaps in the FQH state. At half filling, however, the temperature dependence of conductivity $\sigma(T)$ becomes quite weak, as anticipated for a Fermi sea of composite fermions, and we find a logarithmic dependence of σ on T. The sign of this quantum correction coincides with the weak antilocalization of graphene composite fermions, indigenous to chiral Dirac particles.

DOI: 10.1103/PhysRevB.97.075113

I. INTRODUCTION

The fractional quantum Hall (FQH) state is a many-body phenomenon where fractionally charged elementary excitations lead to quantization of the Hall conductance at a fractional filling factor $\nu = hn/(eB)$ at a carrier density n and magnetic field B [1]. The generation of these incompressible liquid states requires a large Coulomb interaction energy compared with the disorder potential, putting strict requirements on temperature, the quality of the two-dimensional electron gas (2DEG), and the strength of the magnetic field. Owing to reduced screening in atomically thin graphene, the electrons in graphene interact with a larger Coulomb interaction energy than electrons in semiconductor heterostructures, providing an excellent setting for studies of FQH states and their description in terms of composite fermions [2–4].

The composite fermion theory [2] and composite fermion Chern-Simon (CFCS) theory [5–8] have been very successful in outlining a unified picture of the fractional quantum Hall effect. Lopez and Fradkin [5] showed that the problem of interacting electrons moving in 2D in the presence of an external magnetic field is equivalent to a fermion system, described by a Chern-Simon gauge field, where electrons are bound to an even number of vortex lines. Fluctuations in the gauge field were soon realized to have a strong influence on the quantum correction of the composite fermion conductivity [6]. Subsequently, a Fermi-liquid type of theory was proposed for the half-filled Landau level [7] where various observables in the low-temperature limit are described in terms of Fermi-liquid parameters [8], involving most notably the effective mass m^* for composite fermions, which is expected to have a strong enhancement near half filling.

Extensive experimental evidence exists in favor of a weakly interacting Fermi sea of composite fermions effectively in a zero magnetic field at $\nu = 1/2$. Transport anomalies in the lowest Landau level of two-dimensional electrons at half filling were observed by Jiang *et al.* [9]. Distinct features related with compressibility in surface-acoustic-wave propagation on high-quality AlGaAs/GaAs heterostructures were observed by Willett *et al.* [10–12]. Furthermore, resonances at fields where the classical cyclotron orbit becomes commensurate with a superlattice have been found [13,14]. A strong enhancement of the composite fermion mass near $\nu = 1/2$ has been observed in experiments on similar 2DEG heterostructures [15,16]. A logarithmic temperature dependence of conductivity at half-integer filling factors has been observed, which has been interpreted to point towards residual interactions between composite fermions [17–19].

Graphene, owing to the pseudospin originating from the two-atom basis, may display reduced backscattering that will result in weak antilocalization (WAL). This has been observed for Dirac particles in graphene at small magnetic fields [20], and similar WAL behavior might carry over to graphene composite fermions instead of interaction-induced quantum corrections to conductivity [21]. In our present work, we demonstrate experimentally the presence of chiral, Dirac-particle-like composite fermions in monolayer graphene by measuring quantum corrections to conductivity for a half-filled quantum Hall state in magnetic fields of $B = 5$–9 T. By using a micron-wide suspended Corbino disk with high mobility, we find evidence of weak antilocalization behavior at half filling, in spite of the inherent field fluctuations in the composite fermion system. Our results display typical logarithmic temperature corrections for two-dimensional weak localization (WL), but with an opposite sign in comparison to previous observations in 2DEG experiments [18,19].

Interaction and weak localization corrections to conductivity in graphene are influenced by the pseudospin introduced by the two-atom basis of the hexagonal lattice. The pseudospin leads to an additional Berry phase of π in the backscattering wave interference, resulting in reduced backscattering, or in other words, antilocalization [22–24]. True time reversal symmetry (TRS) of graphene requires intervalley scattering, which makes its weak localization phenomena intriguing. In fact, low-field magnetoresistance in graphene may be either positive or negative, depending on the strength of the intervalley and dephasing scattering, as well as on the rate for TRS breaking in a single valley [20,24,25].

In the composite fermion picture, a charge carrier is combined with two flux lines, vortices. The underlying valley

structure will be reflected on the graphene composite fermions, and we expect scattering processes with similar relations among the graphene composite fermions as for graphene Dirac particles at small fields. Consequently, quantum corrections to conductivity at $\nu = 1/2$ can be either positive (WAL) or negative (WL) depending on the rates of intervalley, dephasing, and single-valley TRS breaking scattering for composite fermions denoted as τ_i^{-1}, τ_φ^{-1}, and τ_*^{-1}, respectively. Even though fluctuations due to Chern-Simon fields will enhance the dephasing rate of composite carriers, we anticipate the tendency towards weak antilocalization to remain, which reflects the presence of a Berry phase due to the Dirac nature of these composite carriers.

Recently, Corbino geometry was used in graphene experiments which focused on studies of magnetoconductance in the quantum Hall regime [26,27]. These previous measurements on graphene Corbino disks have failed to show any FQH states, perhaps due to the strong charge inhomogeneity induced by the substrate. Our experiments at mK temperatures, however, display a multitude of FQH states in the lowest Landau level which are clearly visible in magneto- and transconductance measurements [28]. In our devices, conductance is governed by bulk properties instead of the chiral edge states of regular quantum Hall bars. Consequently, a current-annealed, suspended graphene Corbino disk forms an excellent system to study carrier dynamics in the free Fermi sea of composite fermions at half filling.

II. METHODS

The samples considered here are denoted by EV2 ($r_o = 1900$ nm, $r_i = 750$ nm), EV3 ($r_o = 1600$ nm, $r_i = 400$ nm), and C2 ($r_o = 1400$ nm, $r_i = 450$ nm), where r_o and r_i denote the outer and inner radii of the Corbino disks. Our sample fabrication is explained in detail in Ref. [28]. First, we exfoliated graphene on LOR (lift-off resist) using a heat-assisted exfoliation technique to maximize the size of the exfoliated flakes [29]. The contacts were deposited by employing poly(methyl methacrylate) (PMMA)-based lithography in a scheme developed further from the ideas presented in Ref. [30]. A strongly doped silicon Si^{++} substrate with 285 nm of thermally grown SiO_2 was used as a global back gate. Annealing of samples on LOR was typically performed at low temperatures using a bias voltage of 1.6 ± 0.1 V, which is comparable with our HF etched, rectangular two-lead samples [31,32].

In our suspended devices (see Fig. 1), the Corbino disk is supported only by the inner and outer leads made of Au/Cr [28]. The conductivity was calculated from the measured conductance G using $\sigma = \frac{G}{2\pi} \ln(r_o/r_i)$. The field-effect mobility was determined using the equation $\mu_f = \frac{\sigma - \sigma_0}{ne}$ after subtracting out the contact resistance from σ and the measured minimum conductivity σ_0 at the Dirac point ($V_g = V_g^d \sim -2$ V). Our samples had $\mu_f \simeq 1.3$–2×10^5 cm^2/V s at low n. The residual charge density $n_0 \simeq 1$–2×10^9 cm^{-2} for the best regions of the samples was identified by looking for a crossover between constant and power-law behavior in log G vs log n traces in the unipolar transport regime. Contact doping [32] is estimated to correspond to a charge density of $n_c \sim 5\times10^{11}$ cm^{-2} under the contact metal. Details concerning the determination of these basic parameters are given in Ref. [28].

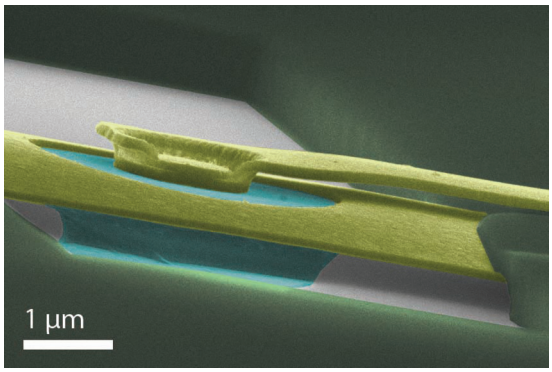

FIG. 1. False-color scanning electron micrograph of a typical sample. The teal circular ring is the graphene sheet, yellow parts denote the gold contacts, dark green marks the LOR support, and the underlying substrate appears as gray.

The zero-B conductance of graphene in Corbino geometry at V_g^d is equal to $G = \frac{8e^2}{h} \log(\frac{r_o}{r_i})^{-1}$ according to the conformal mapping theory [33]. After subtraction of the contact resistance, our measured conductivity is in line with the above theoretical value, as well as with the predicted chemical potential dependence [33]. Also, the measured gate voltage dependence of $G(V_g)$ in the unipolar regime was found to agree with the theoretical formula, which at the same time gave an estimate $R_c = 410\ \Omega$ for the contact resistance. The high sample quality is also manifested in the observability of broken symmetry states ($\nu = 0,3,4$) down to 0.6 T.

Our measurements down to 20 mK were performed on a BlueFors LD-400 dilution refrigerator. The measurement lines were equipped with three-stage RC filters containing $R = 150\ \Omega$ and $C = 10$ nF. Because of the large RC time constant, $\sim$1 s at 30 MΩ sample resistance, most of the magnetoconductance measurements, illustrated in Fig. 2 for the sample EV2, were performed at dc using appropriate

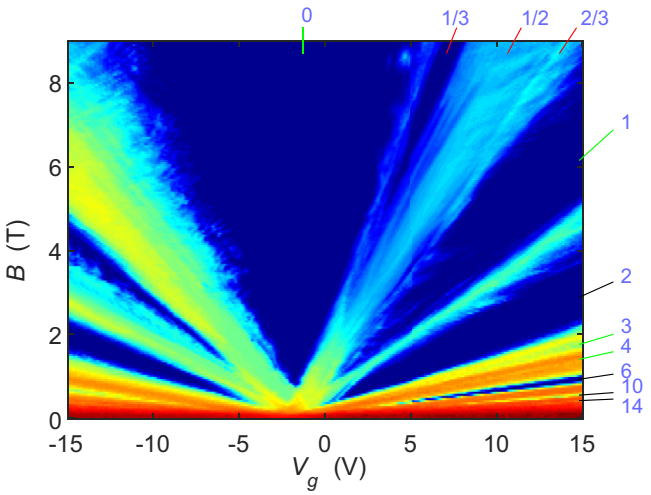

FIG. 2. The magnetoconductance of sample EV2 displayed as a Landau fan diagram on the B vs gate voltage V_g plane; data measured at $f = 3.333$ Hz using ac peak-to-peak excitation current $I_{p\text{-}p} = 0.1$ nA at 20 mK. The region of half filling is given by the slope 0.64 T/V starting from the zero-field Dirac point at $V_g = -2.3$ V.

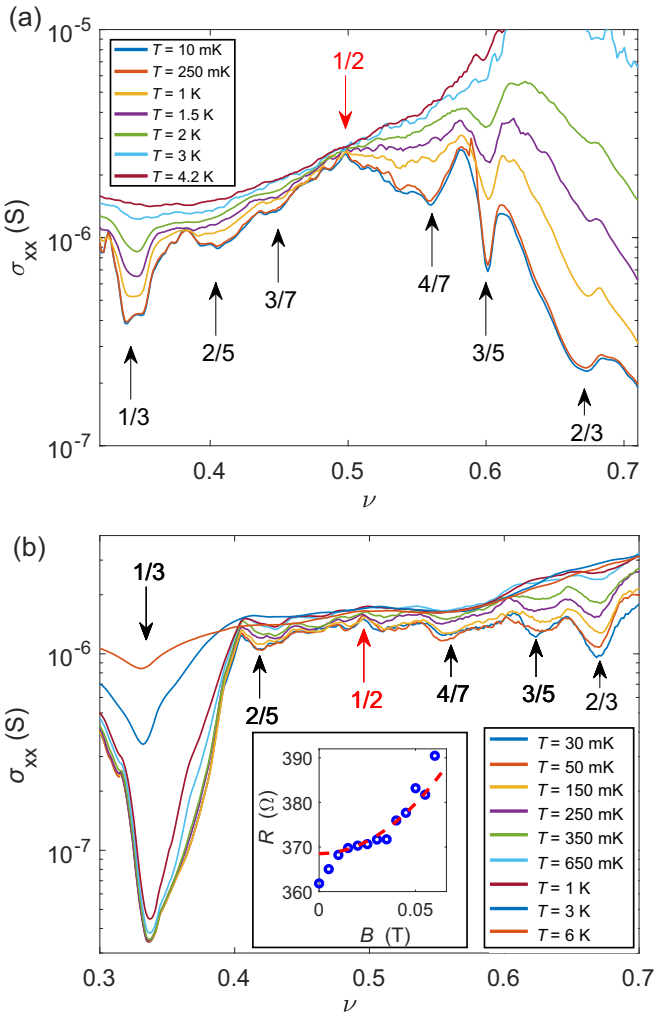

FIG. 3. Temperature dependence of the dc conductivity for the Corbino samples (a) EV3 at $B = 5$ T measured over the charge density $n = 3.8$–8.6×10^{10} cm^{-2} (V_g up to 8.3 V), and (b) EV2 at $B = 9$ T measured over the charge density $n = 6.5$–15.2×10^{10} cm^{-2} (V_g up to 13.9 V). The main FQH states are marked using black arrows in both pictures. The inset of (b) displays the magnetoresistance of the sample EV3 near zero real field $B = 0$ T at $V_g = 10$ V. The dashed red line denotes a guide to the eyes based on classical magnetoresistance of the form $R(B) = R_0 + aB^2$.

waiting times up to 5 s (for $G > 2\times10^{-8}$ S). Since the symmetry of the Corbino geometry enforces the azimuthal electric field to zero, our experiment is sensitive only to the longitudinal conductivity σ_{xx} of the sample.

III. MAGNETOCONDUCTANCE AROUND 1/2 FILLING

Our data on the electronic conductivity σ_{xx} versus the gate-swept filling factor $\nu = hn/(eB)$ in sample EV3 are displayed in Fig. 3(a) for several temperatures in the range $T = 0.01$–4.2 K measured at $B = 5$ T. Similar data from the sample EV2 in the temperature range $T = 0.03$–6 K at $B = 9$ T are displayed in Fig. 3(b). In both cases the half-filling regime is characterized by the weakest temperature dependence of σ_{xx}, which is in accordance with the absence of any energy gap in this regime. Only a linear background variation of $\sigma_{xx}(\nu)_{|6K}$ around $\nu = 1/2 \equiv hn/eB_{1/2}$ is observed at the highest measured temperatures, which indicates washing out of quantum corrections to conductance by thermal fluctuations.

The effective field seen by the composite fermions is given by $\overline{B} = B - B_{1/2}$, which amounts to $\overline{B} = 0$ at $\nu = 1/2$. From the data in Fig. 3 we see that the magnetoconductance around $\overline{B} = 0$ is negative at the lowest mK temperatures. This negative magnetoconductance with respect to $\overline{B}$ applies to all our samples at the magnetic fields $5\,\mathrm{T} < B < 9$ T. Foremost, however, this work deals with the transport behavior at $B = 9$ T, at which the composite fermion effects and the FQH states are the clearest. The main characteristics of the data around half filling at 9 T can be summarized by $d\sigma_{xx}/dT > 0$ and $d\sigma_{xx}/d|\overline{B}| < 0$. The regime of $d\sigma_{xx}/d|\overline{B}| < 0$ covers only the range $\nu \simeq 0.49$–0.51 which corresponds to effective fields $|\overline{B}| < 200$ mT.

The temperature dependence of σ_{xx} can also be employed to determine the energy gaps E_g/k_B around $\nu = 1/2$, for which we obtain, at 5 T, $(B - 2hn/e)\times3$ K/T $- \Gamma_0$ and $(B - 2hn/e)\times6$ K/T $- \Gamma_0$ with $\Gamma_0 \sim 1$–2 K for particles and holes, respectively. Using the slopes $dE_g/d\nu$ and the relation $B_{\mathrm{eff}} = hn/(e\nu)(1 - 2\nu)$ at a fixed magnetic field, we obtain for the effective masses $0.4m_e$ and $0.8m_e$ at fields at $B_{\mathrm{eff}} > 0$ and at $B_{\mathrm{eff}} < 0$, respectively, where m_e denotes the electron mass [34]. In graphene, the cyclotron mass increases with charge density as $n^{1/2}$. We find an even faster, approximately linear, increase in the composite fermion m^* with n at $B_{\mathrm{eff}} < 0$ while this is absent at $B_{\mathrm{eff}} > 0$.

For a comparison of the magnetoconductivity in Fig. 3 at small $\overline{B}$ with phenomena observed at small B, we note that there may be either positive or negative magnetoresistance in graphene around $B = 0$ T [24]. The sign of the magnetoresistance has been demonstrated to depend fundamentally on the parameters τ_φ/τ_i and τ_φ/τ_*; when both of these values are $\lesssim 1$, weak antilocalization is preferred and $d\sigma/dT < 0$ [20]. In Ref. [20], small ratios were achieved at elevated temperatures $T \gg 4.2$ K. In our suspended sample, we were able to observe WAL even at 20 mK, and the range of weak antilocalization magnetoconductance was found to be within $\delta B = 10$–20 mT [see the inset of Fig. 3(b)]. At high B, the magnetoconductance measurements as a function of $|\overline{B}|$ are complicated by the gauge field variation $\sim$100 mT originating from charge variation via the composite fermion flux attachment.

IV. DISCUSSION

Figure 4 displays the temperature dependence of conductivity σ_{xx} for samples EV2 and EV3 at $\nu = 1/2$. The data indicate $\sigma_{xx} = \lambda\frac{e^2}{h}\log T + \mathrm{const}$ with an increase in σ_{xx} with temperature where $\lambda = 0.005$. For our third sample C2, we found similar behavior with $\lambda = 0.008$. Altogether, the observed quantum correction is quite large and it amounts to $\sim$20% of σ_{xx} over the measured range.

To relate the measured conductivity to the properties of composite fermions, we follow the treatment given in Ref. [2] for 2DEG composite fermions (for alternate views, see also Refs. [35–37]). Then, the connection between electronic conductivity σ_{xx} in units e^2/h and the (scaled) composite fermion

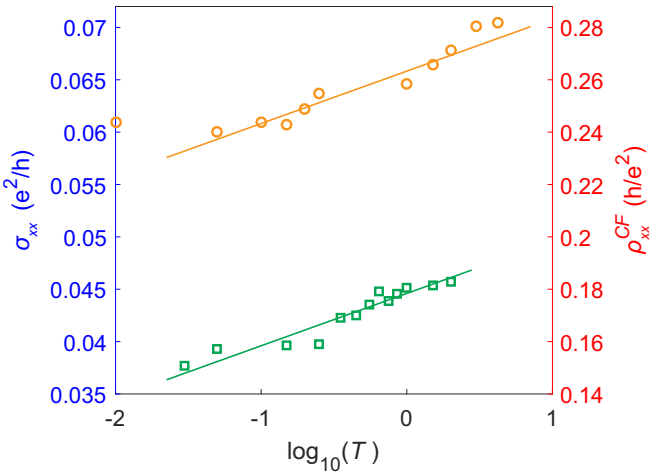

FIG. 4. Temperature dependence of conductivity σ_{xx} for samples EV2 (green squares) and EV3 (orange circles) at half filling $\nu = 1/2$ prepared at $B = 9$ T and $B = 5$ T, respectively; the right axis denotes the resistivity of the composite fermions ρ_{xx}^{CF} obtained from σ_{xx} using the transformation given by Eq. (1) at the limit $\rho_{xx}^{\mathrm{CF}} \ll 1$. The lines correspond to the logarithmic quantum correction in ρ_{xx}^{CF} calculated using $\lambda_\rho = 0.02$ (see text).

resistivity ρ_{xx}^{CF} is given by

$$\sigma_{xx} = \frac{\rho_{yy}^{\mathrm{CF}}}{4 + \rho_{xx}^{\mathrm{CF}}\rho_{yy}^{\mathrm{CF}}}, \tag{1}$$

where the factor of four appears from the off-diagonal elements of the Chern-Simon resistivity matrix. Equation (1) has been employed to extract $\rho_{xx}^{\mathrm{CF}} = \rho_{yy}^{\mathrm{CF}}$ of the composite fermions.

It is expected [2] that $\rho_{xx}^{\mathrm{CF}} \ll 1$. Consequently, we obtain a simple conversion rule: $\rho_{xx}^{\mathrm{CF}} = 4\sigma_{xx}$. The resulting resistivity ρ_{xx}^{CF} for composite fermions is indicated on the right axis in Fig. 4. Since the logarithmic dependence for composite fermions turned into resistivity, the sign of the quantum correction is now reversed, and we are dealing with antilocalization of composite fermions: The prefactor of the logarithmic correction term for resistivity $\rho_{xx}^{\mathrm{CF}} = \lambda_\rho \frac{h}{e^2} \log T + \mathrm{const}$ becomes $\lambda_\rho = +0.02$. This means a different sign when compared with previous observations on 2D electron gas systems with composite fermions at $\nu = 1/2$ [17–19]. One possible explanation for this different behavior is that Chern-Simon field fluctuations suppress very strongly the weak localization contributions in regular 2D electron gas, leaving only interaction corrections to conductivity, whereas weak antilocalization effects due to pseudospin still survive in graphene.

In the presence of impurity scattering, the composite fermion motion will be cut off by a finite transport mean free path ℓ. For $q \ll 2/\ell$, the random phase approximation result is $\sigma_{xx} = \frac{2}{k_F \ell}\frac{e^2}{(2p)^2 h}$, where $2p$ indicates the number of vortices connected to each electron [3]. By fitting this formula to our data on sample EV3 using $p = 1$, we obtain $k_F \ell \simeq 12$ (8.8), which yields $\ell \sim 250$ nm (150 nm) for the mean free path of composite fermions at $B = 5$ T ($B = 9$ T). This indicates clearly diffusive motion as $\ell \ll L$. However, the impurity concentration in our sample does not coincide with this mean free path, and we conclude that this scattering length is set by the Chern-Simon field fluctuations. At 5–9 T fields, we find approximately $\ell \propto 1/B$.

The combined effect of the diffusive motion of composite fermions and the gauge field interaction has been studied by Khveshchenko [38,39] and by Mirlin and Wölfle [40]. In addition to the weak localization/antilocalization contributions, the magnetoresistance may be influenced by the localization of charge carriers due to the magnetic field fluctuations that lead to cyclotron radii which allow closed loops for orbiting particles to be formed. Reference [41] considers magnetic field fluctuations of magnitude of B_0 and correlation length d with a scaled correlation function specified as $\langle B(r)B(0)\rangle = B_0^2 F(r/d)$. Depending on whether $d/R_0 = \alpha \lessgtr 1$, i.e., the ratio of the correlation radius to the cyclotron radius R_0 in the field B_0, their analysis deals with weak or strong random magnetic field (RMF) fluctuations, respectively. We estimate the correlation radius $d \sim 100$ nm as it is related to the size of charge puddles which in high-quality graphene may be on the order of 100 nm [42]. In the text below we will argue that $B_0 \simeq 100$ mT is supported by our results. Consequently, $\alpha \sim 2$ and we are in the intermediate-α regime, but closer to strong RMF fluctuations. Based on an analysis of snake states and localized trajectories [43] at $\alpha \gg 1$, Ref. [41] obtains for conductance $\sim k_F d/\alpha^{1/2}$. Thus, σ_{xx} should enhance approximately as $n^{1/2}$ as B is increased at $\nu = 1/2$, provided that the correlation radius d remains unchanged. Our data for samples EV2 and EV3 at fixed $\nu = 1/2$ follow a sum of a constant+linear increase in σ_{xx} with increasing n above ~3 and ~4 T, respectively, which is in agreement with a linearized form of the theoretical $n^{1/2}$ dependence.

At $\nu \neq 1/2$, there will be a nonzero average field $\overline{B}$ seen by the composite fermions. If $\overline{B}$ is so large that the cyclotron radius is clearly smaller than d, the majority of the trajectories become localized. The localization of composite fermions leads to a reduction in the number of the charge carriers, which diminishes conduction across the Corbino sample. This will lower the conductivity σ_{xx} of the sample as seen in Fig. 4 around $\nu = 1/2$. The amount of localized trajectories for $\alpha \sim 1$ increases quickly when the field $\overline{B}$ seen by the composite fermions becomes $\sim B_0$. Thus, a decrease in conductivity is obtained at effective fields $\overline{B} > B_0$ [41]. By looking at the decay range of σ_{xx} around $\nu = 1/2$ at 9 T in Fig. 3(b), we obtain an estimate of $B_0 \simeq 100$ mT. This is quite close to the RMF variation magnitude given by $n_0 \frac{2h}{e} \sim 75$–150 mT. Therefore, we conclude that the negative, classical magnetoconductance around $\nu = 1/2$ dominates over the weak antilocalization corrections seen in $\sigma_{xx}(T)$ at $\nu = 1/2$.

Our suspended graphene samples always contain built-in nonuniform strain, which can result in visible frozen ripples at room temperature. This strain is modified by the applied gate voltage, which can induce additional rippling around the perimeter if the graphene sheet is able to slide against the metallic contact. A variation in strain in suspended graphene will lead to locally varying pseudomagnetic fields that will lead to dephasing and TRS-breaking scattering within one cone (i.e., shorten τ_φ and τ_*). According to Ref. [25], nonuniform strain is the main contributor to both elastic scattering time τ and τ_*, and $\tau \simeq \tau_*$ within a factor of 2–3. This scenario explains the observation of WAL also in our sample at $B \simeq 0$.

Using similar arguments as above, Chern-Simon fluctuations governing ρ_{xx}^{CF} will strongly enhance scattering rates

τ^{-1}, τ_φ^{-1}, and τ_*^{-1} at $\nu = 1/2$ at high fields. Typically, it is argued that weak localization effects cannot be observed in the presence of Chern-Simon field fluctuations that have an infrared divergence in the density of states of low-frequency excitations at small wave vectors q [8]. In our sample, however, there is a rather high infrared cutoff due to a small geometrical size and low carrier density. By taking a cutoff $q_{\min} \simeq 1/(r_o - r_i)$ and $k_F = \sqrt{\pi n}$, we obtain for the ratio $q_{\min}/k_F \simeq 0.01$ at $n \simeq 10^{11}$ cm^{-2}. Consequently, the Chern-Simon fields do not kill the weak localization effects of graphene composite fermions, but rather just reduce the dephasing time (and the ratios τ_φ/τ_* and τ_φ/τ_i) which favors weak antilocalization behavior among graphene Dirac particles [20].

V. CONCLUSIONS

In conclusion, we have investigated fractional quantum Hall states in a suspended graphene Corbino disk around half filling. We find a weak logarithmic temperature dependence of conductivity, the sign of which indicates a weak antilocalization behavior of graphene composite fermions. These observations with nearly zero effective field acting on composite fermions can be understood by drawing a parallel with the weak antilocalization theories of graphene Dirac particles at small magnetic fields and using classical arguments to analyze the role of gauge field fluctuations in magnetoconductance.

ACKNOWLEDGMENTS

We thank A. Harju, Y. Meir, T. Ojanen, S. Paraoanu, and E. Sonin for fruitful discussions. This work has been supported in part by the EU Framework Programme (H2020 Graphene Flagship) and the European Research Council (Grant No. 670743), and by the Academy of Finland (Grants No. 250280 and No. 286098).

[1] D. C. Tsui, H. L. Stormer, and A. C. Gossard, Phys. Rev. Lett. **48**, 1559 (1982).
[2] J. K. Jain, Phys. Rev. Lett. **63**, 199 (1989).
[3] J. K. Jain, *Composite Fermions* (Cambridge University Press, Cambridge, UK, 2007).
[4] J. K. Jain, Annu. Rev. Condens. Matter Phys. **6**, 39 (2015).
[5] A. Lopez and E. Fradkin, Phys. Rev. B **44**, 5246 (1991).
[6] V. Kalmeyer and S. C. Zhang, Phys. Rev. B **46**, 9889 (1992).
[7] B. I. Halperin, P. A. Lee, and N. Read, Phys. Rev. B **47**, 7312 (1993).
[8] S. H. Simon, in *Composite Fermions*, edited by O. Heinonen (World Scientific, Singapore, 1998), pp. 91–194.
[9] H. W. Jiang, H. L. Stormer, D. C. Tsui, L. N. Pfeiffer, and K. W. West, Phys. Rev. B **40**, 12013 (1989).
[10] R. L. Willett, M. A. Paalanen, R. R. Ruel, K. W. West, L. N. Pfeiffer, and D. J. Bishop, Phys. Rev. Lett. **65**, 112 (1990).
[11] R. L. Willett, R. R. Ruel, M. A. Paalanen, K. W. West, and L. N. Pfeiffer, Phys. Rev. B **47**, 7344 (1993).
[12] R. L. Willett, in *Composite Fermions* (Ref. [8]), pp. 349–442.
[13] W. Kang, H. L. Stormer, L. N. Pfeiffer, K. W. Baldwin, and K. W. West, Phys. Rev. Lett. **71**, 3850 (1993).
[14] H. Deng, Y. Liu, I. Jo, L. N. Pfeiffer, K. W. West, K. W. Baldwin, and M. Shayegan, Phys. Rev. Lett. **117**, 096601 (2016).
[15] H. C. Manoharan, M. Shayegan, and S. J. Klepper, Phys. Rev. Lett. **73**, 3270 (1994).
[16] R. R. Du, H. L. Stormer, D. C. Tsui, A. S. Yeh, L. N. Pfeiffer, and K. W. West, Phys. Rev. Lett. **73**, 3274 (1994).
[17] W. Kang, S. He, H. L. Stormer, L. N. Pfeiffer, K. W. Baldwin, and K. W. West, Phys. Rev. Lett. **75**, 4106 (1995).
[18] L. P. Rokhinson, B. Su, and V. J. Goldman, Phys. Rev. B **52**, R11588 (1995).
[19] L. P. Rokhinson and V. J. Goldman, Phys. Rev. B **56**, R1672 (1997).
[20] F. V. Tikhonenko, A. A. Kozikov, A. K. Savchenko, and R. V. Gorbachev, Phys. Rev. Lett. **103**, 226801 (2009).
[21] D. V. Khveshchenko, Phys. Rev. B **75**, 153405 (2007).
[22] H. Suzuura and T. Ando, Phys. Rev. Lett. **89**, 266603 (2002).
[23] D. V. Khveshchenko, Phys. Rev. Lett. **97**, 036802 (2006).
[24] E. McCann, K. Kechedzhi, V. I. Fal'ko, H. Suzuura, T. Ando, and B. L. Altshuler, Phys. Rev. Lett. **97**, 146805 (2006).
[25] N. J. G. Couto, D. Costanzo, S. Engels, D.-K. Ki, K. Watanabe, T. Taniguchi, C. Stampfer, F. Guinea, and A. F. Morpurgo, Phys. Rev. X **4**, 041019 (2014).
[26] Y. Zhao, P. Cadden-Zimansky, F. Ghahari, and P. Kim, Phys. Rev. Lett. **108**, 106804 (2012).
[27] E. C. Peters, A. J. M. Giesbers, M. Burghard, and K. Kern, Appl. Phys. Lett. **104**, 203109 (2014).
[28] M. Kumar, A. Laitinen, and P. Hakonen, arXiv:1611.02742.
[29] Y. Huang, E. Sutter, N. N. Shi, J. Zheng, T. Yang, D. Englund, H. J. Gao, and P. Sutter, ACS Nano **9**, 10612 (2015).
[30] N. Tombros, A. Veligura, J. Junesch, J. J. van den Berg, P. J. Zomer, M. Wojtaszek, I. J. V. Marun, H. T. Jonkman, and B. J. van Wees, J. Appl. Phys. **109**, 93702 (2011).
[31] A. Laitinen, M. Oksanen, A. Fay, D. Cox, M. Tomi, P. Virtanen, and P. J. Hakonen, Nano Lett. **14**, 3009 (2014).
[32] A. Laitinen, G. S. Paraoanu, M. Oksanen, M. F. Craciun, S. Russo, E. Sonin, and P. Hakonen, Phys. Rev. B **93**, 115413 (2016).
[33] A. Rycerz, P. Recher, and M. Wimmer, Phys. Rev. B **80**, 125417 (2009).
[34] D. Yoshioka, *The Quantum Hall Effect* (Springer, Berlin, 2002).
[35] S. A. Kivelson, D.-H. Lee, Y. Krotov, and J. Gan, Phys. Rev. B **55**, 15552 (1997).
[36] N. Nagaosa and H. Fukuyama, J. Phys. Soc. Jpn. **67**, 3353 (1998).
[37] D. T. Son, Phys. Rev. X **5**, 031027 (2015).
[38] D. V. Khveshchenko, Phys. Rev. Lett. **77**, 362 (1996).
[39] D. V. Khveshchenko, Phys. Rev. B **55**, 13817 (1997).
[40] A. D. Mirlin and P. Wölfle, Phys. Rev. B **55**, 5141 (1997).
[41] A. D. Mirlin, D. G. Polyakov, and P. Wolfle, Phys. Rev. Lett. **80**, 2429 (1998).
[42] J. Xue, J. Sanchez-Yamagishi, D. Bulmash, P. Jacquod, A. Deshpande, K. Watanabe, T. Taniguchi, P. Jarillo-Herrero, and B. LeRoy, Nat. Mater. **10**, 282 (2011).
[43] D. K. K. Lee, J. T. Chalker, and D. Y. K. Ko, Phys. Rev. B **50**, 5272 (1994).